JACS Au
AN OPEN ACCESS JOURNAL OF THE AMERICAN CHEMICAL SOCIETY

pubs.acs.org/jacsau

Article

Pattern Recognition of microRNA Expression in Body Fluids Using Nanopore Decoding at Subfemtomolar Concentrations

Nanami Takeuchi, Moe Hiratani, and Ryuji Kawano*

Cite This: https://doi.org/10.1021/jacsau.2c00117

Read Online

ACCESS | Metrics & More | Article Recommendations | Supporting Information

ABSTRACT: This paper describes a method for detecting microRNA (miRNA) expression patterns using the nanopore-based DNA computing technology. miRNAs have shown promise as markers for cancer diagnosis due to their cancer type specificity, and therefore simple strategies for miRNA pattern recognition are required. We propose a system for pattern recognition of five types of miRNAs overexpressed in bile duct cancer (BDC). The information of miRNAs from BDC is encoded in diagnostic DNAs (dgDNAs) and decoded electrically by nanopore analysis. With this system, we succeeded in the label-free detection of miRNA expression patterns from the plasma of BDC patients. Moreover, our dgDNA−miRNA complexes can be detected at subfemtomolar concentrations, which is a significant improvement compared to previously reported limits of detection (~10^{-12} M) for similar analytical platforms. Nanopore decoding of dgDNA-encoded information represents a promising tool for simple and early cancer diagnosis.

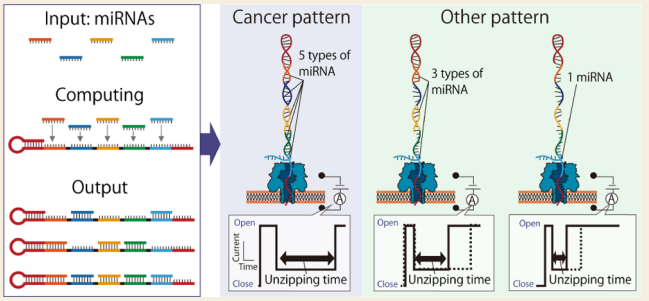

KEYWORDS: *DNA computing technology, nanopore, microRNA, cancer, membrane*

INTRODUCTION

DNA computing uses the biochemical reactions of information-encoding DNA molecules to solve problems. The autonomous calculations are implemented in parallel in a wet environment. Initially, DNA computing was developed largely as a curiosity-driven exercise focused on solving mathematics-related problems. The power of DNA computing was first demonstrated in the early pioneering work of Adleman in 1994,[1] in which he presented a method to solve the Hamiltonian path problem—a mathematical problem also known as the traveling salesman problem. After proposing this groundbreaking idea, extensive methods of DNA computation have been studied, including logic gates.[2] The logic operation has been one of the most attractive informational processes for DNA computation, given that logic operations are constructed by simple binary combinations of OR, NOT, and AND gates, for instance. This method allows higher-level calculations to be performed by combining a number of logic gates, with any logic gate capable of construction by combining multiple NAND (negative-AND) gates.[3]

In conventional DNA computation, the recognition of output molecules is mainly performed by combining several methodologies such as gel electrophoresis or fluorescence detection, followed by polymerase chain reaction (PCR) amplification.[1,4,5] To improve the speed of decoding, we have recently proposed nanopore decoding for the detection of the output molecules directly and electrically. We constructed several logic gates including AND, OR, NOT, and NAND, and the output molecule was detected by nanopore measurement of the electrical signals in a droplet-based nanopore device.[6−9] In addition, we have also studied nanopore decoding for solving the Hamiltonian path problem with parallel computation, as mentioned above.[10] Based on experiences from these previous studies, we are convinced that nanopore decoding is appropriate for rapid and simple decoding in DNA computing.

Recently, the potential of DNA computing in medical diagnostics has also been realized.[11] Benenson et al. reported autonomous diagnosis and drug-release systems with DNA computing using the following "if-then" logic: "if" certain diagnostic conditions are true, such as low expression levels of certain mRNAs relative to those of others, "then" the antisense drug is released.[12] After this pioneering study, several studies were undertaken focused on the application of this technology to diagnosis and therapy. Based on the favorable compatibility of nanopore technology with oligonucleotide detection,[13−15] strategies utilizing this method for diagnosis using nanopores and DNA have been proposed.[16] MicroRNA, which is a short noncoding RNA that has about 18−25 nucleotides, is an important target in terms of diagnosis for cancers because its

Received: February 22, 2022
Revised: May 23, 2022
Accepted: May 24, 2022

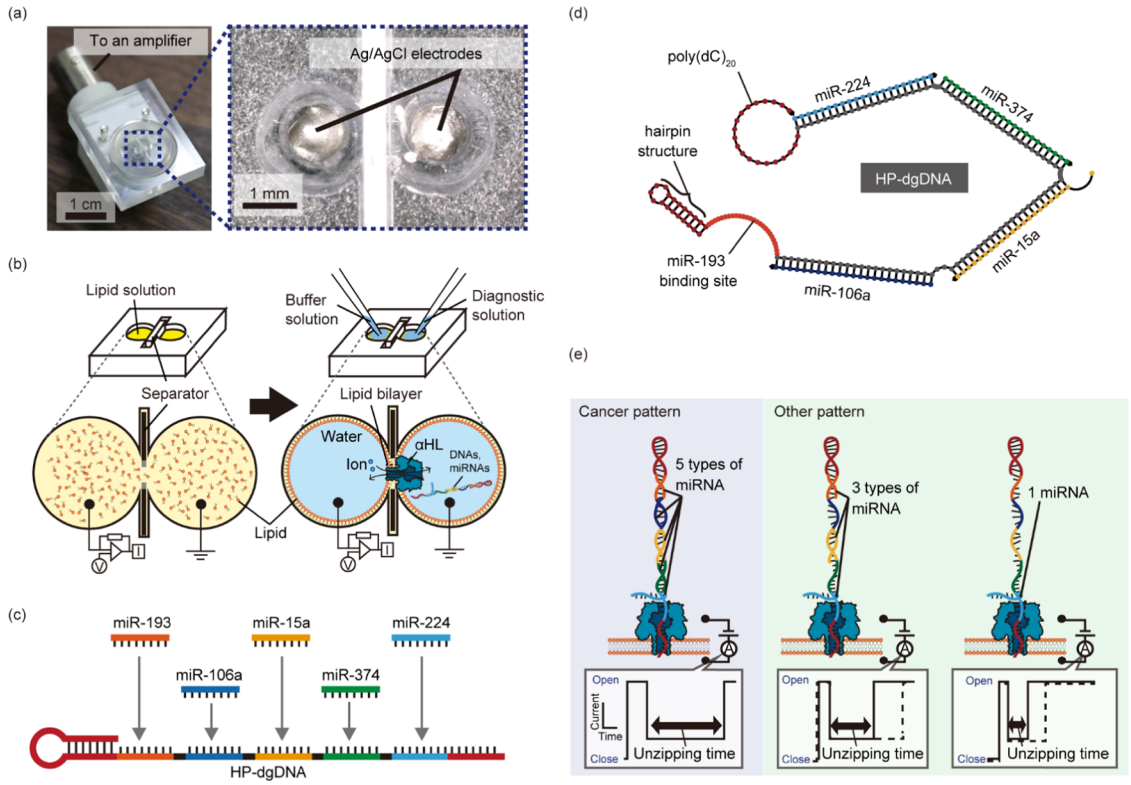

Figure 1. Design of the miRNA detection system using DNA computing technology and nanopore decoding. (a) Photograph of the device used for nanopore analysis. (b) Schematic illustration of lipid bilayer preparation. (c) Design of HP-dgDNA. (d) Structure of the duplex of HP-dgDNA and miR-193, miR-106a, miR-15a, and miR-374, simulated by NUPACK. When we simulated the structure, we converted the sequence of HP-dgDNA into the corresponding RNA sequence and replaced the "A" of HP-dgDNA sequence with "U". (e) Schematic illustration of the technical principle of nanopore decoding of HP-dgDNA.

expression is regulated with cancer types from early stages, and the high-cancer specificity of the pattern of miRNA expression is attracting attention as a form of liquid biopsy.[17−27] In recent years, several approaches based on logic operations have been developed, including conventional DNA computation and gold nanoparticle strategies.[28,29] We have also constructed the AND gate for the detection of two overexpressed miRNAs (miR-20a and miR-17-5p) that are secreted from small cell lung cancer (SCLC).[30] In this system, two diagnostic DNAs were encapsulated in input droplets and formed a four-way junction with the miRNAs only when the two miRNAs were present at the same time (equivalent to an AND gate operation). The structure of the four-way junction blocked the nanopore and generated a long current inhibition as the output signal, resulting in current block durations specific for each system of (1, 1), (0, 1), (1, 0), and (0, 0). This logic operation enables simple and rapid diagnostic applications using nanopore analysis. However, although parallel operation is the most intriguing characteristic of DNA computing, implementing logic operations in multiplex diagnosis remains an unsolved challenge.

Here, we report a method for the identification of the expression patterns of five different types of miRNAs (miR-193, miR-106a, miR-15a, miR-374, and miR-224) based on DNA computing combined with nanopore decoding. These miRNAs are overexpressed in bile duct cancer (BDC), which is one of the highest mortality cancers.[31,32] A diagnostic DNA with a hairpin structure (HP-dgDNA), which has the ability to detect multiple miRNAs simultaneously, is employed as the computational molecule. By forming a duplex structure with the five miRNAs, HP-dgDNA performs information processing to convert the expression pattern of the miRNAs into a nucleic acid structure that can be decoded using the nanopore. During translocation through the pore, the hybridized miRNAs will be "unzipped" from the diagnostic DNA, which will result in a current inhibition of characteristic amplitude and duration. We analyzed the unzipping time of the miRNA pattern and were able to recognize the BDC-specific expression pattern of the miRNAs even from clinical samples. In addition, we found that our method can detect the miRNA pattern at the attomolar (10^{-18} M) level using an excess of the HP-dgDNA.

MATERIAL AND METHOD

Reagents and Chemicals

All aqueous solutions were prepared with ultrapure water from a Milli-Q system (Millipore, Billerica, MA). The reagents were as follows: 1,2-diphytanoyl-*sn*-glycero-3-phosphocholine (DPhPC; Avanti Polar Lipids, Alabaster, AL), *n*-decane (Wako Pure Chemical Industries, Ltd., Osaka, Japan), potassium chloride (KCl; Nacalai Tesque), 3-(*N*-morpholino)-propanesulfonic acid (MOPS; Nacalai Tesque, Kyoto, Japan). Wild-type α-hemolysin (αHL; List Biological Laboratories, Campbell, CA and Sigma-Aldrich, St Louis, MO) was obtained as a monomer polypeptide, isolated from *Staphylococcus aureus* in powder form, and dissolved at a concentration of 1 mg/mL in ultrapure water. For use, samples were diluted to the designated concentration using a buffered electrolyte solution and stored at 4 °C. High-performance liquid chromatography (HPLC)-grade DNA oligonucleotides and miRNA were

https://doi.org/10.1021/jacsau.2c00117
JACS Au XXXX, XXX, XXX−XXX

synthesized by FASMAC Co., Ltd. (Kanagawa, Japan) and stored at −20 and −80 °C, respectively.

Patients and Healthy Samples

Plasma samples were supplied by a biobank operated by the National Center for Global Health and Medicine (Tokyo, Japan). Patient samples were obtained from six patients with histologically proven BDC. All of the samples were obtained from patients who had undergone surgical resection in May 2010−November 2016. The diagnosis of these patients was based on histological assessment after surgical resection. Additionally, plasma samples were collected from 11 healthy volunteers (HVs) and the plasma of 6 HVs was pooled for analysis. The clinicopathological backgrounds of the patients and HVs are shown in Supporting Information Table S1. After sample collection, blood samples were centrifuged at 3000 rpm for 10 min at 15 °C to spin down the blood cells. Plasma samples were then transferred into fresh collection tubes and stored at −80 °C until further processing.

Small RNA Extraction

Small RNAs were extracted from 300 μL of plasma with a NucleoSpin miRNA Plasma (Takara Bio, Inc., Shiga, Japan) according to the manufacturer's protocol. At the beginning of each extraction procedure, exogenous control cel-miR-39-3p (FASMAC) was spiked into samples before the addition of lysis buffer. The final volume was 30 μL. All eluted RNA samples were stored at −80 °C until used.

Quantification of miRNA by Quantitative Real-Time PCR (RT-qPCR)

Amounts of miRNAs were quantified by quantitative real-time PCR (RT-qPCR) using the SYBR Advantage qPCR Premix (Takara). The reverse transcription reaction was carried out with the Mir-X miRNA First-Strand Synthesis Kit (Takara) according to the manufacturer's instructions. Quantitative PCR was performed on the Thermal Cycler Dice Real-Time System Lite (Takara), and reaction mixtures were incubated at 95 °C for 10 s, followed by 40 cycles at 95 °C for 5 s and 65 °C for 25 s. The cycle threshold (C_t) values were calculated with Multiplate RQ (Takara).

miRNA/HP-dgDNA Hybridization

Diagnostic solutions consisted of each extracted miRNA with 500 nM HP-dgDNA in MOPS buffer (pH 7.0, 10 mM) containing 1 M potassium chloride. These solutions were heated to 95 °C for 5 min and then cooled to room temperature gradually.

Preparation of the Microdevice for Nanopore Analysis

The microdevice used for nanopore analysis was fabricated by machining a 6.0 mm thick, 10 × 10 mm polymethyl methacrylate (PMMA) plate (Mitsubishi Rayon, Tokyo, Japan) using a computer-aided design and computer-aided manufacturing three-dimensional modeling machine (MM-100, Modia Systems, Japan). Two wells (2.0 mm in diameter and 4.5 mm in depth) and a chase between the wells were manufactured on the PMMA plate. Each well had a through-hole in the bottom, through which Ag/AgCl electrodes were installed to the bottom of the wells (Figure 1a). A polymeric film made of parylene C (polychloro-*p*-xylylene) with a thickness of 5 μm was patterned with a single pore (100 μm in diameter) using a conventional photolithography method and then fixed between PMMA films (0.2 mm thick) using an adhesive (Super X, Cemedine Co., Ltd, Tokyo, Japan). The films, including the parylene film, were inserted into the chase to separate the wells.

Bilayer Lipid Membrane (BLMs) Preparation and Reconstitution of αHL

Bilayer lipid membranes (BLMs) were prepared using the microdevice fabricated as described above (Figure 1a). BLMs can be spontaneously formed in this device by the droplet contact method (Figure 1b).[6,7,33] In this method, the two lipid monolayers contact each other and form BLMs on the 100 μm aperture in the parylene C film that separates the two wells. BLMs were formed as follows: the wells of the device were filled with *n*-decane (2.5 μL) containing DPhPC (10 mg/mL). Next, the aqueous recording solutions (4.7 μL, 1 M KCl, and 10 mM MOPS, pH 7.0) were added to both of the wells. αHL was reconstituted in BLMs to form a nanopore from the ground side. The diagnostic solution after miRNAs/HP-dgDNA hybridization was also added to the ground side. Within a few minutes of adding the solutions, BLMs were formed and αHL reconstructed nanopores within them. If the BLMs ruptured during this process, they were recreated by tracing with a hydrophobic stick at the interface of the droplets.

Channel Current Measurements and Data Analysis

The channel current was recorded with an Axopatch 200B amplifier (Molecular Devices), filtered with a low-pass Bessel filter at 10 kHz with a sampling rate of 50 kHz. A constant voltage of +200 mV was applied from the recording side, while the other side was grounded. The recorded data from Axopatch 200B were acquired with Clampex 9.0 software (Molecular Devices) through a Digidata 1440A analog-to-digital converter (Molecular Devices). Data were analyzed using Clampfit 10.6 (Molecular Devices), Excel (Microsoft, Washington), and Origin Pro 8.5J (Light Stone, Tokyo, Japan). DNA or miRNA translocation and blocking were detected when >80% of open αHL channel currents were inhibited. Between 251 and 322 translocating or blocking events were recorded. From these data, we generated histograms of unzipping time for each sample using a bootstrap method. The event frequency was counted for each 1 min interval when a single αHL pore was open. Nanopore measurements were conducted at 22 ± 2 °C.

Stability Prediction of the miRNA/HP-dgDNA Duplex

The Gibbs free energy (ΔG_{sim}) of each of the miRNA/HP-dgDNA duplex was predicted by the nearest-neighbor (NN) model with NN parameters for RNA/DNA hybrids.[34]

RESULTS

Design of Diagnostic DNA (HP-dgDNA)

We selected miR-193, miR-106a, miR-15a, miR-374, and miR-224 as target miRNAs for BDC diagnosis because these miRNAs have been reported to be overexpressed in human intrahepatic cholangiocarcinoma.[31] We designed HP-dgDNA, a diagnostic DNA with a hairpin structure and a sequence that enables the linear binding of all of the five target miRNAs (Figure 1c and Supporting Information Table S2). The detailed design rationale is as follows:

(i) The complementary strands of the five miRNAs are inserted into the main sequence to encode the miRNA patterns (dgDNA).
(ii) Poly$(dC)_{20}$ is added at the 3′ end of dgDNA to be exclusively inserted into αHL pore. The length of

https://doi.org/10.1021/jacsau.2c00117
JACS Au XXXX, XXX, XXX−XXX

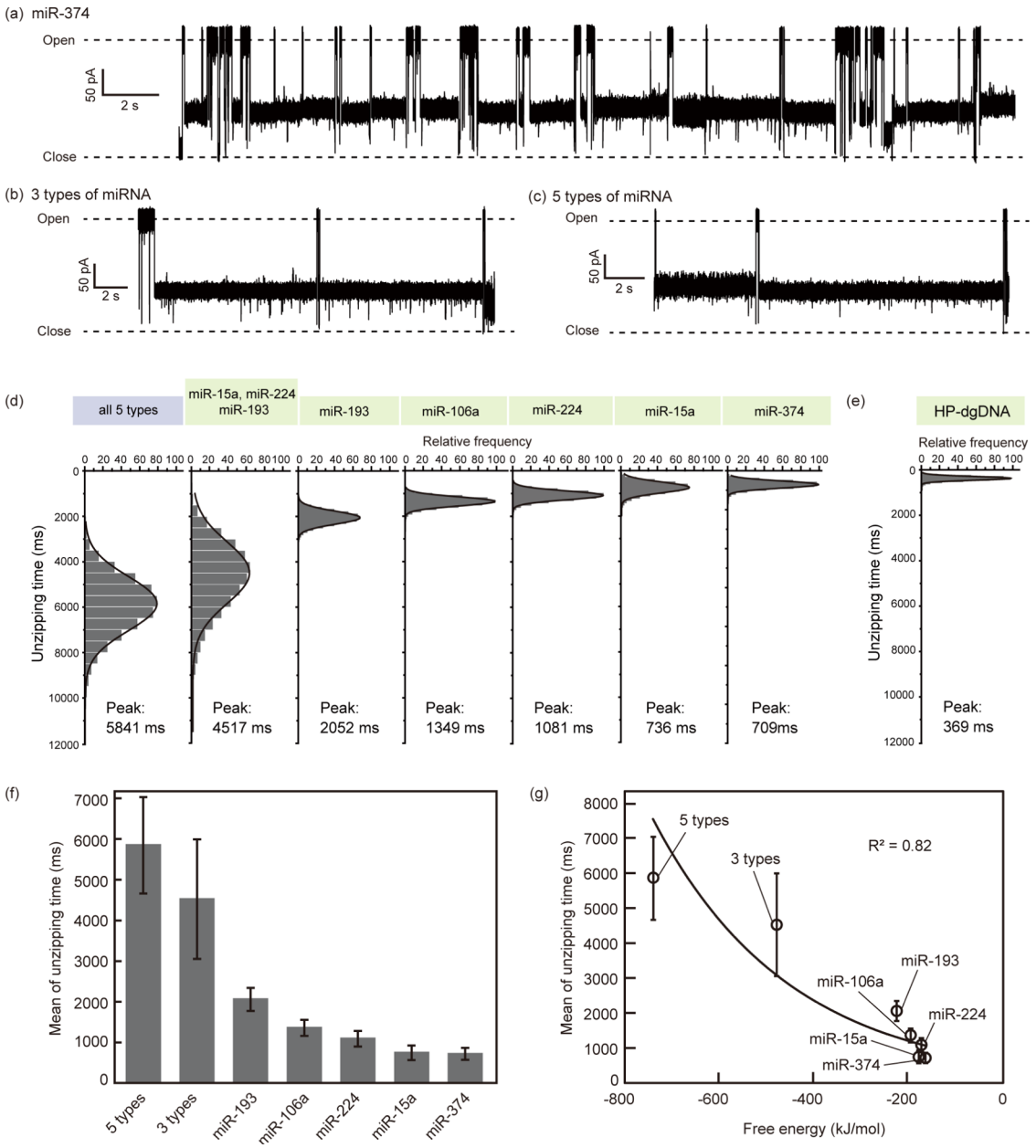

Figure 2. Results of nanopore analysis of each miRNA pattern. (a)−(c) Characteristic current signals of different combinations of miRNAs bound to HP-dgDNA: (a) miR-374; (b) miR-15a, miR-224, and miR-193; and (c) miR-15a, miR-224, miR-193, miR-106a, and miR-374. (d) Histograms of unzipping time of each miRNA pattern. (e) Histogram of unzipping time of translocation of HP-dgDNA without bound miRNAs. (f) Mean of the unzipping time of each miRNA pattern. (g) Mean of the unzipping time as a function of the free energy of each duplex of HP-dgDNA and miRNAs. Error bars represent the mean ± standard deviation (SD) after the bootstrap analysis.

poly(dC)$_{20}$ is 8.4 nm; therefore, the HP-dgDNA can penetrate the αHL pore because the length from the entrance to the β-barrel structure of the pore is 4.8 nm.

(iii) The HP-dgDNA hairpin structure is added at the 5′ end of dgDNA to prevent insertion into the αHL pore from the 5′ end.[35]

All designed structures were checked by thermodynamic simulation (NUPACK: http://www.nupack.org/, and nearest-neighbor (NN) model). The duplex formation of HP-dgDNA and the miRNAs at 500 nM each were simulated thermodynamically (Figure 1d). The NUPACK simulation can calculate ΔG_{sim} of a secondary structure composed of only DNA or RNA alone. Therefore, ΔG_{sim} of RNA/DNA binding was calculated by the NN model using NN parameters.[34] All ΔG_{sim} values of each miRNA/HP-dgDNA hybridization are listed in Supporting Information Table S3.

Two cytosines were set in between the complementary sequence of each miRNA as spacers. The thermodynamic simulation showed that the two-cytosine spacers make the duplex sufficiently stabilized (Supporting Information Figure S1). Next, we determined the order of complementary strands of the five miRNAs in HP-dgDNA using simulations. To inhibit the unpredicted formation of secondary structures, the sequence order was selected to have the smallest hybridization energy from the 120 (=5!) possible sequence orders. The optimal strand order resulted in a minimum ΔG_{sim} of −94.8 kJ/mol (Supporting Information, Figure S2). The HP-dgDNA

https://doi.org/10.1021/jacsau.2c00117
JACS Au XXXX, XXX, XXX−XXX

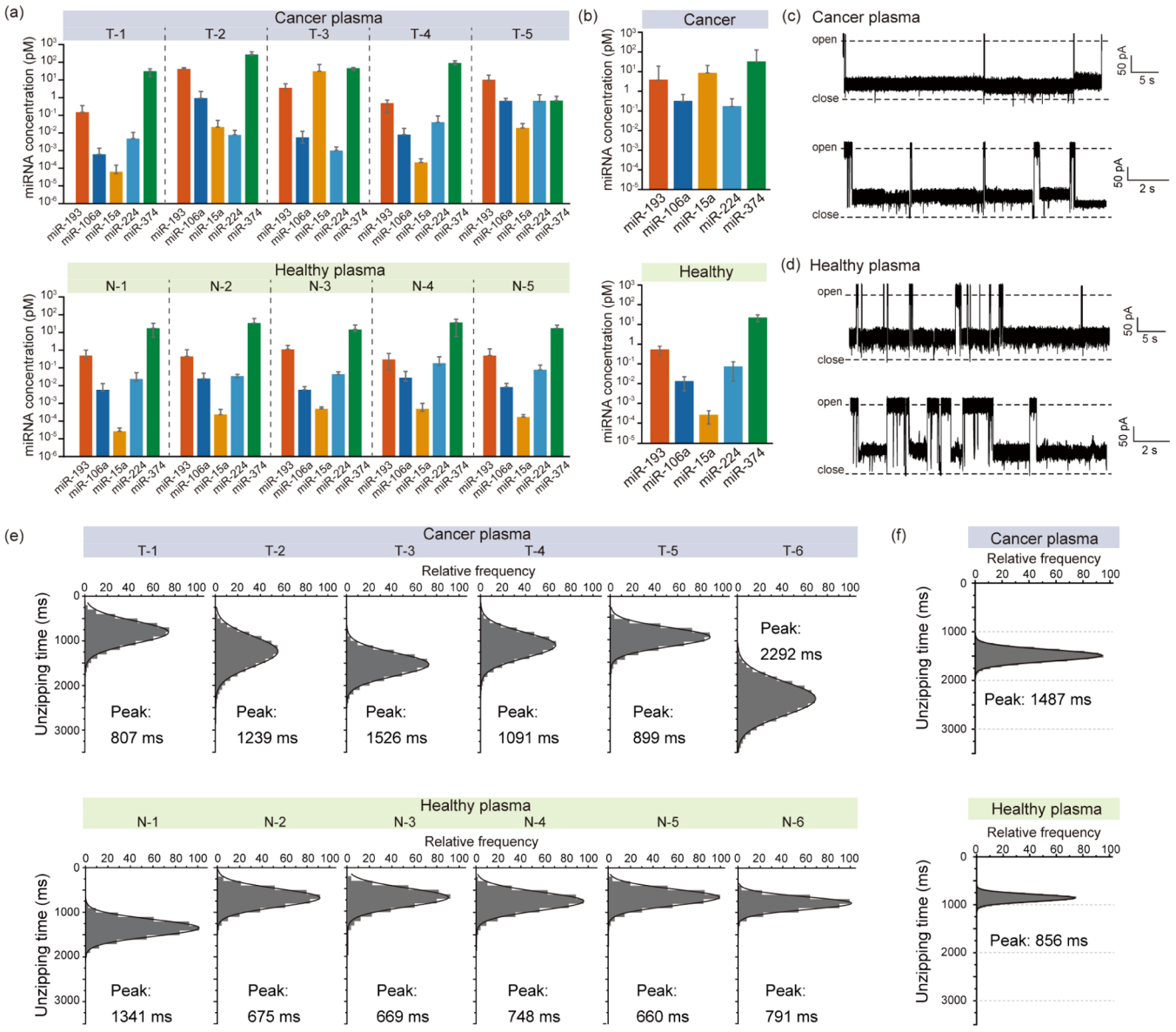

Figure 3. Results of RT-qPCR and nanopore analysis of real plasma samples. (a) miRNA concentration of the five cancer patient plasma samples and the five healthy volunteer plasma samples quantified by RT-qPCR. (b) Average miRNA concentration of the five cancer patient samples and the five healthy volunteer samples. Characteristic current signal of cancer patient plasma samples (c) and healthy volunteer plasma samples (d). (e) Histograms of the unzipping time of the six cancer patient samples and the six healthy volunteer samples. (f) Average unzipping time of plasma samples. All error bars are mean ± SE.

structure fulfilling the above requirements is shown in Figure 1c,d.

The long cytosine homo-sequence was selected as the 3′-end-tail because it enables the detection of HP-dgDNA insertion based on the unique current blocking ratio of poly(dC) (I_b = 70%) to open pore current.[36] The blocking ratio of poly(dC) is likely to be higher than 70%, while the blocking ratio of poly(dA) and poly(dT) is likely to be 50%.

Nanopore Analysis of Each miRNA Pattern

In the nanopore analysis of the miRNA/HP-dgDNA duplex, there were two possibilities: that the duplex passed through the nanopore resulting in the unzipping of the complementary strands (Figure 1e) or that the duplex returned to the *cis* solution.[37] To confirm the translocation of HP-dgDNA of the duplex, we measured the complex of miR-193/HP-dgDNA using αHL at 150 or 200 mV (Supporting Information Figure S3a). Histograms of the unzipping time, the duration of unzipping events, were made using the bootstrap method, a statistical method, and the mean value of the unzipping time at 200 mV was shorter than that at 150 mV (Supporting Information, Figure S3b). The unzipping time was shortened by increasing the applied voltage, suggesting that the duplex of miR-193/HP-dgDNA entered the pore was pushed out by the voltage and then passed through the pore with the unzipping of miR-193. The unzipping signal ratio has been reported to become higher with an increase in applied voltage.[38,39] Therefore, to facilitate the unzipping, the applied voltage of 200 mV was adopted for the following experiments.

To validate the proof of concept, we prepared a cancer miRNA pattern (with all 5 miRNAs present) and two healthy miRNA patterns (with 1 or 3 miRNAs present) using synthetic miRNAs. In each pattern, unzipping signals with over 80%

https://doi.org/10.1021/jacsau.2c00117
JACS Au XXXX, XXX, XXX−XXX

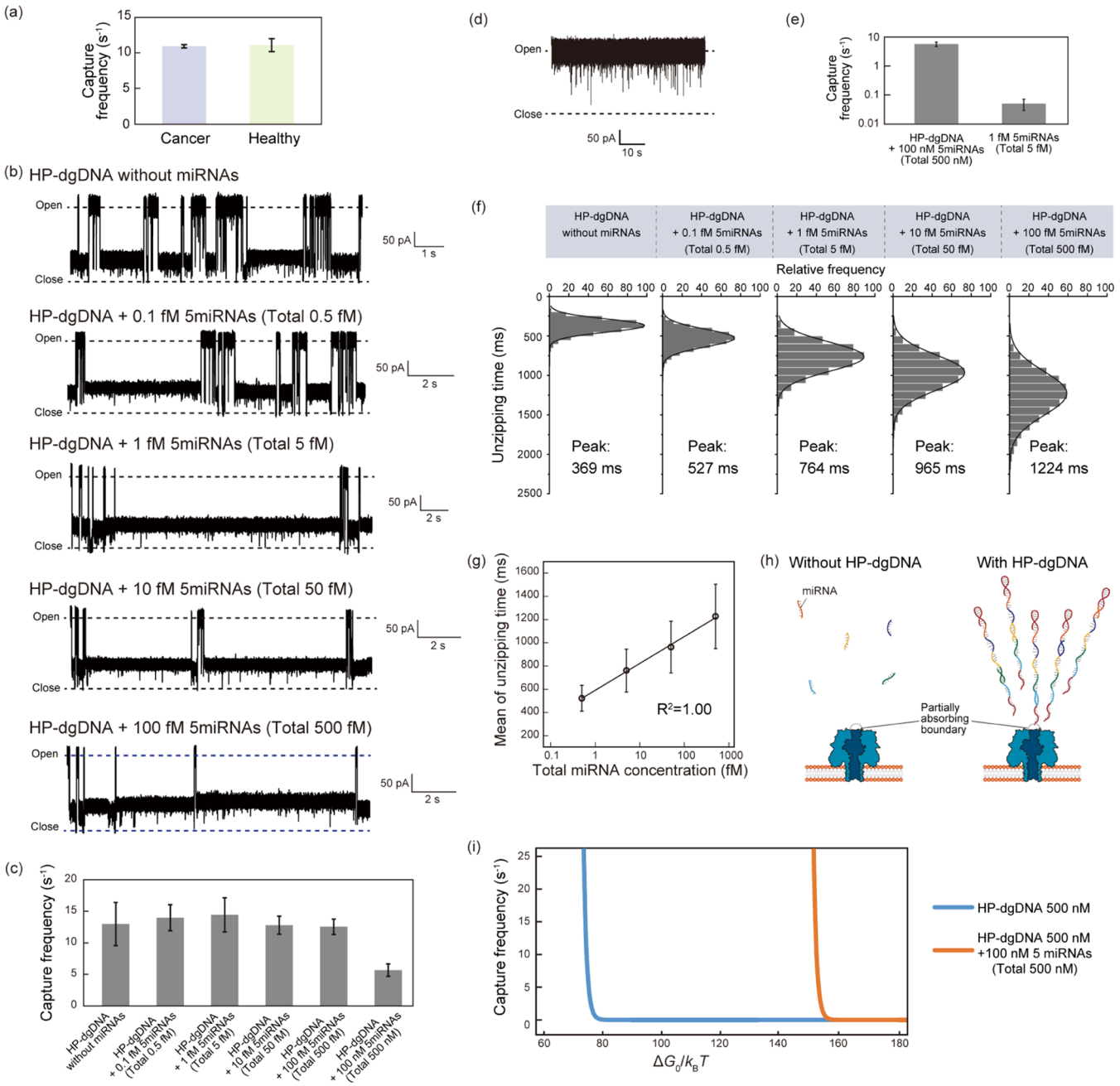

Figure 4. Results of subfemtomolar miRNA detection. (a) Average capture frequency of the six cancer samples and the six healthy samples in the presence of HP-dgDNA. (b) Characteristic current signals of 500 nM HP-dgDNA and miRNAs at each concentration. (c) Capture frequency of 500 nM HP-dgDNA and miRNAs for each condition. Using 5 fM miRNAs without HP-dgDNA, we observed a characteristic signal (d) and its capture frequency (e). (f) Histograms of the unzipping time of each miRNA pattern. HP-dgDNA was 500 nM in each. (g) Mean of the unzipping time as a function of the total miRNA concentrations. All error bars are mean ± SD. (h) Schematic illustration of the femtomolar miRNA detection with/without 500 nM HP-dgDNA. (i) The capture frequency calculated by the theoretical model.

blocking were observed; hence, we propose that HP-dgDNA was inserted from poly(dC)$_{20}$ and subsequently passed through the αHL pore with unzipping of the miRNAs and its hairpin structure (Figure 2a–c). The mean current blocking ratio ($I_{b,mean}$) was [$I_{b,mean}$ ± 2.2%] (n = 37). A previous study showed that the standard error (SE) of the blocking current of poly(dC)$_{50}$ was 2–4%, which is approximately consistent with our result. We analyzed the unzipping time with the assumption that unzipping time reflects the number of miRNAs bound to HP-dgDNA. Histograms of the unzipping time were also made using the bootstrap method (Figure 2d). The peak values of unzipping time histogram of miR-374, miR-15a, miR-224, miR-106a, miR-193, three miRNAs, and five miRNAs were 709, 736, 1081, 1349, 2052, 4517, and 5841 ms, respectively. Each peak value was larger than that of HP-dgDNA itself, at 369 ms (Figure 2e). This result shows that miRNAs were unzipped from HP-dgDNA during the translocation through the αHL pore, with a characteristic unzipping time (Figure 2e). The unzipping time became larger as the number of miRNAs binding to HP-dgDNA increased, and correlated with the ΔG_{sim} of the duplex (Figure 2f,g). In the case of the singly bound miRNA, the unzipping time also

https://doi.org/10.1021/jacsau.2c00117
JACS Au XXXX, XXX, XXX–XXX

became longer with increasing ΔG_{sim} (Figure 2e,f). These results indicate that complexes with a larger ΔG_{sim} require a longer time to be unzipped from HP-dgDNA in the αHL pore. The unzipping time showed an exponential dependence on ΔG_{sim} (R^2 = 0.82), and this result is consistent with previous studies[40,41] (Figure 2g and Supporting Information, Figure S4). Our system could be used to recognize other miRNA patterns of different cancers by adjusting ΔG_{sim} and controlling the unzipping time. Regarding the specificity of this method, there are already several reports on the specificity/selectivity of the hybridization of oligonucleotides including miRNAs.[37,42,43] As demonstrated in several reports of miRNA detection techniques, our system would have enough specificity for miRNAs.[23,44,45]

RT-qPCR of Clinical Samples

Based on the results of the proof-of-concept study, we next attempted to recognize miRNA patterns using clinical plasma samples. The five miRNAs, miR-15a, miR-193, miR-224, miR-106a, and miR-374, are known to be overexpressed in cholangiocytes microdissected from the tissue of BDC patients.[31] To confirm the expression level in plasma before performing the nanopore decoding, absolute quantification of miRNAs extracted from the plasma samples was conducted by RT-qPCR. First, we prepared calibration curves of the five miRNAs and cel-miR-39-3p, as spike-in miRNA (Supporting Information Figure S5). The difference in the efficiency of reverse transcription and amplification between the five miRNAs was normalized using the calibration curves of the five miRNAs. The difference in the efficiency of reverse transcription and amplification between the samples was normalized by the calibration curve of the spike-in miRNA. The miRNA concentration in each of the samples was between approximately 30 aM to 7.0 nM (Figure 3a). To distinguish the cancer patients and the healthy volunteers (HVs), we had to interpret the five-dimensional data (= concentration value of the five miRNAs). One way to distinguish cancer patients from healthy controls using a combination of values attributed to multiple miRNAs is by logistic regression.[46] However, it has been reported that for logistic regression, the sample size should be at least 5 times larger than the explanatory variables.[47] For this study, we would therefore need more than 5 × 5 = 25 samples because there were five types of miRNAs. Since clinical samples of BDC are difficult to obtain due to the small patient numbers in Japan, we instead analyzed the difference in the expression level of each miRNA of the five cancer patients and the five HVs. The concentration of each of the miRNAs in the cancer patients was higher compared to the HVs. In the cancer patients, miR-193, miR-106a, and miR-15a were significantly overexpressed compared to the HVs with $p < 0.01$. Although other two miRNAs (miR-224 and miR-374) did not show a significant difference, the mean concentrations were higher in the cancer patients (Figure 3b and Supporting Information). To the best of our knowledge, this is the first report revealing that the miRNAs known to increase in BDC tissue are also overexpressed in plasma.

Nanopore Analysis of Clinical Samples

HP-dgDNA hybridized with miRNAs extracted from the plasma samples were examined by nanopore analysis. In both cancer and HV samples, over 80% inhibition of the ion current flowing through the pore was observed, as also observed with synthetic miRNAs (Figure 3c,d), indicating that miRNA detection is possible even with the use of clinical samples. It was possible that HP-dgDNA and the five miRNAs comprised 32 ($=2^5$) types of secondary structure in the hybridized combinations with different concentrations. We observed various unzipping times on the order of 10^{-2} to 10^6 ms (Supporting Information Figure S6), probably due to the wide variety of hybridized structures. We assumed that distributions of unzipping time represented the overall miRNA pattern in each sample since we considered the ratio of miRNAs/HP-dgDNA duplex in a crowd of HP-dgDNA to be reflected in the distributions. Therefore, the histogram of the unzipping time was prepared by the bootstrap method, and the peak values of each of the cancer patients and HVs were obtained (Figure 3e). The average unzipping times of the cancer patients and HVs were 1487 ms and 856 ms, respectively (Figure 3f). The miRNA expression level was higher in the cancer patients than in the HVs, a result in line with the RT-qPCR analysis. However, we cannot find a clear relationship between the unzipping time and the total concentration of miRNAs in the plasma sample probably due to the complex binding pattern. The cutoff value of unzipping time to distinguish between cancer patients and HVs calculated in this study was 1011 ms (Supporting Information Figure S7). As a result, our nanopore technique using HP-dgDNA with a multiplexing property distinguished the cancer patients from the HVs without generating a calibration curve for each miRNA.

Investigation of Subfemtomolar Detection with a Model System Using Synthetic miRNAs

Generally, the frequency of DNA/RNA translocation *via* a nanopore (= capture frequency) is used to estimate the detection capability against a target concentration. We also calculated the capture frequency of the plasma samples in addition to the unzipping times. However, as shown in Figure 4a, monitoring the capture frequency did not allow for recognition of the miRNA patterns in the BDC because the HP-dgDNA was present at a higher concentration (500 nM) and therefore dominated the frequency events. To investigate detection at low concentrations, we designed model experiments with similar experimental conditions to the clinical experiments: 0.1, 1, 10, and 100 fM of each of the five miRNAs were used with 500 nM HP-dgDNA and the capture frequency was analyzed (Figure 4b). Although the capture frequencies of the femtomolar conditions were similar to each other, the 500 nM miRNAs/HP-dgDNA duplex showed a lower frequency (Figure 4c). These results suggest that miRNAs/HP-dgDNA with residual HP-dgDNA show higher frequency, and miRNAs/HP-dgDNA itself shows lower frequency. Besides, in the presence of only miRNAs without HP-dgDNA, the frequency of 1 fM 5 miRNAs (total 5 fM) with over 80% inhibition was around 0.05 s^{-1}; this value was less than one-hundredth of 500 nM 5 miRNAs/HP-dgDNA (5.68 s^{-1}, Figure 4d,e).

We next analyzed the unzipping time of the model experiments. The unzipping times of the femtomolar concentrations of miRNAs with 500 nM HP-dgDNA were measured and compared with each other. The unzipping time increased with the increase in the concentration of the miRNAs, suggesting that miRNA can be detected at subfemtomolar concentrations using the HP-dgDNA (Figure 4f,g). The calculated detection limit was 0.3 fM in each miRNA (Supporting Information Figure S8).

https://doi.org/10.1021/jacsau.2c00117
JACS Au XXXX, XXX, XXX−XXX

DISCUSSION

Low-Concentration Detection of miRNA/HP-dgDNA in the Nanopore Measurements

Our results when using clinical samples were a pleasant surprise since nanopore measurements have generally been considered unable to detect nucleic acids at subpicomolar concentrations.[37] To measure the subpicomolar or femtomolar targets, several elaborate methods have been proposed; Wang et al. showed the detection of 0.1 pM miR-155 with the αHL nanopore using asymmetric solution conditions of 0.2 M/3 M (*cis*/*trans*) KCl salt gradient, to increase the capture frequency of the target molecule.[37] Zhang et al. used the αHL nanopore with isothermal amplification of nucleic acids, resulting in the detection of 1 fM miR-20a.[48] In contrast, our method was able to detect subfemtomolar miRNAs directly without any modifications to the basic nanopore detection setup.

We consider that the key to this low-concentration detection is the excess amount of HP-dgDNA as the complementary probe for the target miRNAs. Our results in the *in vitro* experiments support this hypothesis:

(1) In the case of the equimolar condition between the HP-dgDNA and miRNAs or the miRNAs themselves, the total capture frequency is constant or decreased (Figure 4c).
(2) In the case of the excess amount of the HP-dgDNA, the unzipping time showed a linear relationship for concentrations ranging from 0.1 fM to 1 pM (Figure 4g).

Consequently, excess HP-dgDNA surrounding target miRNAs/HP-dgDNA caused an increase in the sensitivity, as schematically shown in Figure 4h. To support this hypothesis from a theoretical view, we referred to a nanopore capture model as we have recently proposed.[49] The modeling of the capture frequency f of a particle captured into a nanopore is described by the following equation

$$\frac{1}{f} = \frac{1}{f_a} + \frac{1}{f_e} \tag{1}$$

with f_a an approach frequency related to the migration of particles from the bulk to the pore inlet and f_e an entrance frequency related to the actual entry of particles into the pore region; f_a and f_e are defined as follows

$$f_a = \frac{2\pi a_2 C_0}{1 - e^{-a_2/r_e D}} \tag{2}$$

with

$$a_2 = \frac{\mu q I}{2\pi\sigma} + \frac{Q_f}{2\pi} \tag{3}$$

where C_0 is the particle concentration, r_e is the pore entrance radius, D denotes the diffusion coefficient, μ is the particle mobility, q is the particle charge, I is the ion current flowing through the pore, σ is the electrolyte conductivity, and Q_f is the volumetric flow rate entering the pore, and

$$f_e = 2\pi C_0 r_e^3 \frac{k_B T}{h} \exp\left[2\varphi(r_e) - \frac{\Delta G_0}{k_B T}\right] \tag{4}$$

where k_B is the Boltzmann constant, T is the temperature, h is Planck's constant, $\varphi(r_e)$ is the dimensionless effective potential evaluated at r_e, and ΔG_0 is the free energy barrier at equilibrium. When calculating f for 5 miRNAs/HP-dgDNA and HP-dgDNA, respectively, the parameters that differ between them are q and ΔG_0. If we first consider q: if the ratio of the 5 miRNAs/HP-dgDNA signal was 10 out of 300 signals for the experiments using 0.5 fM miRNAs, f for 5 miRNAs/HP-dgDNA would become more than 10^6 times larger than that for HP-dgDNA. However, using the elemental charge e in this assumption, we calculated that $q = 270e$ for 5 miRNAs/HP-dgDNA and $q = 160e$ for HP-dgDNA, indicating that q is unlikely to have a significant effect on f. Therefore, we assumed that the free energy barrier at equilibrium ΔG_0 between 5 miRNAs/HP-dgDNA and HP-dgDNA is considerably different and affects f. Although proper modeling to predict ΔG_0 is required, ΔG_0 can be represented as

$$\Delta G_0 = c \times k_B T \tag{5}$$

where c is a target-specific constant. Using this model for our case, we plotted f against $\Delta G_0/k_B T$ ($=c$) in Figure 4i. As a result, c values of ssDNA and dsDNA captured into a nanopore were expected to be significantly different, suggesting that ΔG_0 differs between ssDNA and dsDNA (Figure 4i). Therefore, a large excess of ssDNA could promote the migration of dsDNA to the pore.

CONCLUSIONS

In conclusion, we propose a system for miRNA expression pattern recognition using DNA computing and nanopore decoding. The information encoded in miRNA hybridized to HP-dgDNA is decoded by nanopore sensing in the form of unzipping time of the hybridized strands as the diagnostic construct translocates through the nanopore. We successfully distinguished miRNA expression patterns in clinical plasma samples of bile duct cancer patients and HVs. Our nanopore system was able to detect very low concentrations ($\sim 10^{-16}$ M) of miRNA from the plasma samples, which is a significant improvement compared to the previously reported limit of detections for nanopore analysis of DNA/RNA ($\sim 10^{-12}$ M). Based on a theoretical estimation, we found that the higher concentration of our diagnostic DNA compared to the target RNA molecules plays a critical role in this phenomenon. Our finding should be an intriguing physicochemical phenomenon that has never been proposed, and it will be an important concept for low-concentration detection using the nanopore technology.

Regarding the multiplex of our diagnosis system, this system does not require a calibration curve for the quantification of each miRNA. Certainly, our method is possible to quantify the concentration of miRNAs using a calibration curve for each miRNA (Supporting Information Figure S9), and it can be multiplex using the nanopore array device.[7] This approach is similar to conventional multiplex measurements. For instance, a PCR technique requires a large number of sample tubes, and they need each calibration curve for quantification of miRNAs. In this study, however, the multiplexing property of HP-dgDNA enabled the pattern recognition of the five types of miRNAs with a single device.

The proposed system would be potentially useful for medical applications if this system will integrate into a commercially available nanopore sequencer such as MinION (Oxford Nanopore Technologies). Moreover, several biological nanopores other than αHL have also been used for nanopore sensing.[33,50−56] The nanopore decoding will have the potential to apply to the different types of nanopores.

https://doi.org/10.1021/jacsau.2c00117
JACS Au XXXX, XXX, XXX−XXX

■ ASSOCIATED CONTENT

Supporting Information

The Supporting Information is available free of charge at https://pubs.acs.org/doi/10.1021/jacsau.2c00117.

Additional results of unzipping time and thermodynamic simulation, additional information on miRNA detection methods and DNA computing technique, detailed results of RT-qPCR and nanopore measurement for plasma samples, clinicopathological backgrounds of patients and HVs, and DNA/miRNA sequences (PDF)

■ AUTHOR INFORMATION

Corresponding Author

Ryuji Kawano − *Department of Biotechnology and Life Science, Tokyo University of Agriculture and Technology, Tokyo 184-8588, Japan;* orcid.org/0000-0001-6523-0649; Email: rjkawano@cc.tuat.ac.jp

Authors

Nanami Takeuchi − *Department of Biotechnology and Life Science, Tokyo University of Agriculture and Technology, Tokyo 184-8588, Japan*

Moe Hiratani − *Department of Biotechnology and Life Science, Tokyo University of Agriculture and Technology, Tokyo 184-8588, Japan*

Complete contact information is available at: https://pubs.acs.org/10.1021/jacsau.2c00117

Author Contributions

R.K. conceived the original idea. M.H. designed HP-dgDNA and performed the initial experiments. N.T. performed all of the other experiments and analyses. N.T. and R.K. wrote the entire manuscript. All authors have given approval to the final version of the manuscript.

Notes

The authors declare no competing financial interest.

■ ACKNOWLEDGMENTS

The authors thank A. Tamotsu, A. Tada, and M. Yamaji for constructive discussion and advice on data analysis. The biological samples utilized for this research were provided by the Biobank of National Center for Global Health and Medicine in Japan. This research was partially supported by JSPS KAKENHI Grant Numbers 16H06043 (R.K.), 19H00901 (R.K.), 21H05229 (R.K.), and 21H03143 (N.T.).

■ REFERENCES

(1) Adleman, L. M. Molecular computation of solutions to combinatorial problems. *Science* **1994**, *266*, 1021−1024.

(2) Xu, X. H.; Shang, Y. X.; Liu, F. S.; Jiang, Q.; Ding, B. Q. Logic devices based on nucleic acid self-assembly. *InfoMat* **2021**, *3*, 1070−1082.

(3) Fan, D. Q.; Wang, J.; Wang, E. K.; Dong, S. J. Propelling DNA Computing with Materials' Power: Recent Advancements in Innovative DNA Logic Computing Systems and Smart Bio-Applications. *Adv. Sci.* **2020**, *7*, No. 2001766.

(4) Benenson, Y.; Paz-Elizur, T.; Adar, R.; Keinan, E.; Livneh, Z.; Shapiro, E. Programmable and autonomous computing machine made of biomolecules. *Nature* **2001**, *414*, 430−434.

(5) Chen, Y. Q.; Song, Y. Y.; Wu, F.; Liu, W. T.; Fu, B. S.; Feng, B. K.; Zhou, X. A DNA logic gate based on strand displacement reaction and rolling circle amplification, responding to multiple low-abundance DNA fragment input signals, and its application in detecting miRNAs. *Chem. Commun.* **2015**, *51*, 6980−6983.

(6) Yasuga, H.; Kawano, R.; Takinoue, M.; Tsuji, Y.; Osaki, T.; Kamiya, K.; Miki, N.; Takeuchi, S. Logic Gate Operation by DNA Translocation through Biological Nanopores. *PLoS One* **2016**, *11*, No. e0149667.

(7) Ohara, M.; Takinoue, M.; Kawano, R. Nanopore Logic Operation with DNA to RNA Transcription in a Droplet System. *ACS Synth. Biol.* **2017**, *6*, 1427−1432.

(8) Hiratani, M.; Kawano, R. DNA logic operation with nanopore decoding to recognize microRNA patterns in small cell lung cancer. *Anal. Chem.* **2018**, *90*, 8531−8537.

(9) Ding, T. L.; Yang, J.; Pan, V.; Zhao, N.; Lu, Z. H.; Ke, Y. G.; Zhang, C. DNA nanotechnology assisted nanopore-based analysis. *Nucleic Acids Res.* **2020**, *48*, 2791−2806.

(10) Takiguchi, S.; Kawano, R. Nanopore decoding for a Hamiltonian path problem. *Nanoscale* **2021**, *13*, 6192−6200.

(11) Benenson, Y. Biomolecular computing systems: principles, progress and potential. *Nat. Rev. Genet.* **2012**, *13*, 455−468.

(12) Benenson, Y.; Gil, B.; Ben-Dor, U.; Adar, R.; Shapiro, E. An autonomous molecular computer for logical control of gene expression. *Nature* **2004**, *429*, 423−429.

(13) Tan, C. S.; Fleming, A. M.; Ren, H.; Burrows, C. J.; White, H. S. gamma-Hemolysin Nanopore Is Sensitive to Guanine-to-Inosine Substitutions in Double-Stranded DNA at the Single-Molecule Level. *J. Am. Chem. Soc.* **2018**, *140*, 14224−14234.

(14) Shoji, K.; Kawano, R.; White, R. J. Spatially Resolved Chemical Detection with a Nanoneedle-Probe-Supported Biological Nanopore. *ACS Nano* **2019**, *13*, 2606−2614.

(15) Denuga, S.; Whelan, D. E.; O'Neill, S. P.; Johnson, R. P. Capture and analysis of double-stranded DNA with the α-hemolysin nanopore: Fundamentals and applications. *Electrochem. Sci. Adv.* **2022**, No. e2200001.

(16) Kawano, R. Nanopore Decoding of Oligonucleotides in DNA Computing. *Biotechnol. J.* **2018**, *13*, No. 1800091.

(17) Cui, M. Y.; Wang, H. D.; Yao, X. X.; Zhang, D.; Xie, Y. J.; Cui, R. J.; Zhang, X. W. Circulating MicroRNAs in Cancer: Potential and Challenge. *Front. Genet.* **2019**, *10*, No. 626.

(18) Cai, S.; Pataillot-Meakin, T.; Shibakawa, A.; Ren, R.; Bevan, C. L.; Ladame, S.; Ivanov, A. P.; Edel, J. B. Single-molecule amplification-free multiplexed detection of circulating microRNA cancer biomarkers from serum. *Nat. Commun.* **2021**, *12*, No. 3515.

(19) Liyanage, T.; Masterson, A. N.; Oyem, H. H.; Kaimakliotis, H.; Nguyen, H.; Sardar, R. Plasmoelectronic-Based Ultrasensitive Assay of Tumor Suppressor microRNAs Directly in Patient Plasma: Design of Highly Specific Early Cancer Diagnostic Technology. *Anal. Chem.* **2019**, *91*, 1894−1903.

(20) Wang, H.; Peng, R.; Wang, J. J.; Qin, Z. L.; Xue, L. X. Circulating microRNAs as potential cancer biomarkers: the advantage and disadvantage. *Clin. Epigenet.* **2018**, *10*, No. 59.

(21) Cai, S. L.; Pataillot-Meakin, T.; Shibakawa, A.; Ren, R.; Bevan, C. L.; Ladame, S.; Ivanov, A. P.; Edel, J. B. Single-molecule amplification-free multiplexed detection of circulating microRNA cancer biomarkers from serum. *Nat. Commun.* **2021**, *12*, No. 3515.

(22) Xi, D. M.; Shang, J. Z.; Fang, E. G.; You, J. M.; Zhang, S. S.; Wang, H. Nanopore-Based Selective Discrimination of MicroRNAs with Single-Nucleotide Difference Using Locked Nucleic Acid-Modified Probes. *Anal. Chem.* **2016**, *88*, 10540−10546.

(23) Zhong, W. J.; Yang, Q. F.; Fang, K. R.; Xiao, D.; Zhou, C. S. Current Simultaneous Discrimination of Mismatched MicroRNAs Using Base-Flipping within the alpha-Hemolysin Latch. *ACS Sens.* **2021**, *6*, 4482−4488.

(24) Zhang, X. Y.; Wang, Y.; Fricke, B. L.; Gu, L. Q. Programming Nanopore Ion Flow for Encoded Multiplex MicroRNA Detection. *ACS Nano* **2014**, *8*, 3444−3450.

(25) Ivica, J.; Williamson, P. T. F.; de Planque, M. R. R. Salt Gradient Modulation of MicroRNA Translocation through a Biological Nanopore. *Anal. Chem.* **2017**, *89*, 8822−8829.
(26) Zhang, Y.; Song, P.; Guo, B. Y.; Hao, W. Y.; Liu, L.; Wu, H. C. A bifunctional DNA probe for sensing pH and microRNA using a nanopore. *Analyst* **2020**, *145*, 7025−7029.
(27) Wang, L.; Chen, X. H.; Zhou, S.; Roozbahani, G. M.; Zhang, Y. W.; Wang, D. Q.; Guan, X. Y. Displacement chemistry-based nanopore analysis of nucleic acids in complicated matrices. *Chem. Commun.* **2018**, *54*, 13977−13980.
(28) Zhang, C.; Zhao, Y. M.; Xu, X. M.; Xu, R.; Li, H. W.; Teng, X. Y.; Du, Y. Z.; Miao, Y. Y.; Lin, H. C.; Han, D. Cancer diagnosis with DNA molecular computation. *Nat. Nanotechnol.* **2020**, *15*, 709−715.
(29) Liu, L.; Li, N.; Huang, Z. M.; Tang, L. J.; Ying, Z. M.; Jiang, J. H. Gold Nanoflares with Computing Function as Smart Diagnostic Automata for Multi-miRNA Patterns in Living Cells. *Anal. Chem.* **2020**, *92*, 10925−10929.
(30) Hiratani, M.; Ohara, M.; Kawano, R. Amplification and Quantification of an Antisense Oligonucleotide from Target microRNA Using Programmable DNA and a Biological Nanopore. *Anal. Chem.* **2017**, *89*, 2312−2317.
(31) Chen, L.; Yan, H. X.; Yang, W.; Hu, L.; Yu, L. X.; Liu, Q.; Li, L.; Huang, D. D.; Ding, J.; Shen, F.; Zhou, W. P.; Wu, M. C.; Wang, H. Y. The role of microRNA expression pattern in human intrahepatic cholangiocarcinoma. *J. Hepatol.* **2009**, *50*, 358−369.
(32) Sirica, A. E.; Gores, G. J.; Groopman, J. D.; Selaru, F. M.; Strazzabosco, M.; Wang, X. W.; Zhu, A. X. Intrahepatic Cholangiocarcinoma: Continuing Challenges and Translational Advances. *Hepatology* **2019**, *69*, 1803−1815.
(33) Watanabe, H.; Gubbiotti, A.; Chinappi, M.; Takai, N.; Tanaka, K.; Tsumoto, K.; Kawano, R. Analysis of Pore Formation and Protein Translocation Using Large Biological Nanopores. *Anal. Chem.* **2017**, *89*, 11269−11277.
(34) Banerjee, D.; Tateishi-Karimata, H.; Ohyama, T.; Ghosh, S.; Endoh, T.; Takahashi, S.; Sugimoto, N. Improved nearest-neighbor parameters for the stability of RNA/DNA hybrids under a physiological condition. *Nucleic Acids Res.* **2020**, *48*, 12042−12054.
(35) Vercoutere, W.; Winters-Hilt, S.; Olsen, H.; Deamer, D.; Haussler, D.; Akeson, M. Rapid discrimination among individual DNA hairpin molecules at single-nucleotide resolution using an ion channel. *Nat. Biotechnol.* **2001**, *19*, 248−252.
(36) Butler, T. Z.; Gundlach, J. H.; Troll, M. Ionic current blockades from DNA and RNA molecules in the alpha-hemolysin nanopore. *Biophys. J.* **2007**, *93*, 3229−3240.
(37) Wang, Y.; Zheng, D. L.; Tan, Q. L.; Wang, M. X.; Gu, L. Q. Nanopore-based detection of circulating microRNAs in lung cancer patients. *Nat. Nanotechnol.* **2011**, *6*, 668−674.
(38) Mathé, J.; Visram, H.; Viasnoff, V.; Rabin, Y.; Meller, A. Nanopore unzipping of individual DNA hairpin molecules. *Biophys. J.* **2004**, *87*, 3205−3212.
(39) Wang, Y.; Tian, K.; Hunter, L. L.; Ritzo, B.; Gu, L. Q. Probing molecular pathways for DNA orientational trapping, unzipping and translocation in nanopores by using a tunable overhang sensor. *Nanoscale* **2014**, *6*, 11372−11379.
(40) Liu, P.; Kawano, R. Recognition of Single-Point Mutation Using a Biological Nanopore. *Small Methods* **2020**, *4*, No. 2000101.
(41) Ohara, M.; Sekiya, Y.; Kawano, R. Hairpin DNA Unzipping Analysis Using a Biological Nanopore Array. *Electrochemistry* **2016**, *84*, 338−341.
(42) Xu, J. S.; Liao, K. L.; Fu, Z. H.; Xiong, Z. F. A new method for early detection of pancreatic cancer biomarkers: detection of microRNAs by nanochannels. *Artif. Cells, Nanomed., Biotechnol.* **2019**, *47*, 2634−2640.
(43) Gopinath, S. C. B.; Perumal, V.; Xuan, S. J. MicroRNA-155 complementation on a chemically functionalized dual electrode surface for determining breast cancer. *3 Biotech* **2020**, *10*, No. 270.
(44) Zheng, W. L.; Yao, L.; Teng, J.; Yan, C.; Qin, P. Z.; Liu, G. D.; Chen, W. Lateral flow test for visual detection of multiple MicroRNAs. *Sens. Actuators, B* **2018**, *264*, 320−326.
(45) Chandrasekaran, A. R.; MacIsaac, M.; Dey, P.; Levchenko, O.; Zhou, L. F.; Andres, M.; Dey, B. K.; Halvorsen, K. Cellular microRNA detection with miRacles: microRNA-activated conditional looping of engineered switches. *Sci. Adv.* **2019**, *5*, No. eaau9443.
(46) Yokoi, A.; Yoshioka, Y.; Hirakawa, A.; Yamamoto, Y.; Ishikawa, M.; Ikeda, S.; Kato, T.; Niimi, K.; Kajiyama, H.; Kikkawa, F.; Ochiya, T. A combination of circulating miRNAs for the early detection of ovarian cancer. *Oncotarget* **2017**, *8*, 89811−89823.
(47) Vittinghoff, E.; McCulloch, C. E. Relaxing the rule of ten events per variable in logistic and Cox regression. *Am. J. Epidemiol.* **2007**, *165*, 710−718.
(48) Zhang, H. L.; Hiratani, M.; Nagaoka, K.; Kawano, R. MicroRNA detection at femtomolar concentrations with isothermal amplification and a biological nanopore. *Nanoscale* **2017**, *9*, 16124−16127.
(49) Chinappi, M.; Yamaji, M.; Kawano, R.; Cecconi, F. Analytical Model for Particle Capture in Nanopores Elucidates Competition among Electrophoresis, Electroosmosis, and Dielectrophoresis. *ACS Nano* **2020**, *14*, 15816−15828.
(50) Shimizu, K.; Mijiddorj, B.; Usami, M.; Mizoguchi, I.; Yoshida, S.; Akayama, S.; Hamada, Y.; Ohyama, A.; Usui, K.; Kawamura, I.; Kawano, R. De novo design of a nanopore for single-molecule detection that incorporates a beta-hairpin peptide. *Nat. Nanotechnol.* **2022**, *17*, 67−75.
(51) Miyagi, M.; Takiguchi, S.; Hakamada, K.; Yohda, M.; Kawano, R. Single polypeptide detection using a translocon EXP2 nanopore. *Proteomics* **2022**, *22*, No. e2100070.
(52) Zhang, S. L.; Huang, G.; Versloot, R. C. A.; Bruininks, B. M. H.; de Souza, P. C. T.; Marrink, S. J.; Maglia, G. Bottom-up fabrication of a proteasome-nanopore that unravels and processes single proteins. *Nat. Chem.* **2021**, *13*, 1192−1199.
(53) Li, M. Y.; Ying, Y. L.; Yu, J.; Liu, S. C.; Wang, Y. Q.; Li, S.; Long, Y. T. Revisiting the Origin of Nanopore Current Blockage for Volume Difference Sensing at the Atomic Level. *JACS Au* **2021**, *1*, 967−976.
(54) Jia, W. D.; Hu, C. Z.; Wang, Y. Q.; Gu, Y. M.; Qian, G. R.; Du, X. Y.; Wang, L. Y.; Liu, Y.; Cao, J.; Zhang, S. Y.; Yan, S. H.; Zhang, P. K.; Ma, J.; Chen, H. Y.; Huang, S. Programmable nano-reactors for stochastic sensing. *Nat. Commun.* **2021**, *12*, No. 5811.
(55) Robertson, J. W. F.; Ghimire, M. L.; Reiner, J. E. Nanopore sensing: A physical-chemical approach. *Biochim. Biophys. Acta, Biomembr.* **2021**, *1863*, No. 183644.
(56) Jeong, K. B.; Luo, K.; Lee, H.; Lim, M. C.; Yu, J.; Choi, S. J.; Kim, K. B.; Jeon, T. J.; Kim, Y. R. Alpha-Hederin Nanopore for Single Nucleotide Discrimination. *ACS Nano* **2019**, *13*, 1719−1727.

https://doi.org/10.1021/jacsau.2c00117
JACS Au XXXX, XXX, XXX−XXX